ADVANCED FUNCTIONAL MATERIALS
www.afm-journal.de

# High-Entropy Magnetism of Murunskite

*Davor Tolj, Priyanka Reddy, Ivica Živković, Luka Akšamović, Jian Rui Soh, Kamila Komędera, Izabela Biało, Naveen Kumar Chogondahalli Muniraju, Trpimir Ivšić, Mario Novak, Oksana Zaharko, Clemens Ritter, Thomas LaGrange, Wojciech Tabiś, Ivo Batistić, László Forró,* Henrik M. Rønnow,* Denis K. Sunko,* and Neven Barišić**

**Murunskite ($K_2FeCu_3S_4$) bridges the two known families of high-temperature superconductors, cuprates and iron-pnictides, structurally and electronically. Like these families, murunskite exhibits an antiferromagnetic (AF)-like response with an ordered phase below 97 K. The magnetic iron atoms are randomly distributed over one-quarter of the sites in two-dimensional planes, while the remaining sites are occupied by non-magnetic copper, evoking the notion of a high-entropy magnetic alloy. This intriguing magnetic transition is studied by neutron, Mössbauer, and X-ray photoelectron spectroscopy (XPS) measurements on single crystals. The AF order has a nearly commensurate quarterzone wave vector. In the paramagnetic state, Mössbauer spectroscopy identifies two iron sites, associated with $Fe^{3+}$ or $Fe^{2+}$ oxidation states as observed by XPS, which merge into a third site upon cooling, indicating an orbital transition. This cascade of local transitions transforms iron atoms from a fully orbitally and magnetically disordered state to a homogeneously ordered state in inverse space, while still being randomly distributed in real space. This finding challenges the traditional paradigm of magnetism in insulators, which relies on a direct connection between crystal structure and the location of magnetic moments.**

## 1. Introduction

The concept of emergent order is a fundamental preoccupation in contemporary science.[1,2] This phenomenon refers to the spontaneous formation of complex structures and patterns from seemingly disordered systems. Emergent order often arises from the intricate interplay of various physical forces, leading to hierarchical structures and complex behaviors that are not apparent from the individual components. By exploring how order emerges from disorder, scientists aim to uncover the principles that govern the behavior and properties of complex materials and systems.

Modern functional materials, such as high-temperature superconducting compounds, exemplify this concept. These materials, including cuprates and pnictides, exhibit a fascinating blend of chemical and physical electronic properties.[3–7] While chemical binding typically closes electronic

D. Tolj
William H. Miller III Department of Physics and Astronomy
Johns Hopkins University
Baltimore MD 21218, USA

D. Tolj, I. Živković, J. R. Soh, H. M. Rønnow
Laboratory for Quantum Magnetism
École Polytechnique Fédérale de Lausanne
Lausanne CH-1015, Switzerland
E-mail: henrik.ronnow@epfl.ch

P. Reddy, M. Novak, I. Batistić, D. K. Sunko, N. Barišić
Department of Physics
Faculty of Science
University of Zagreb
Zagreb 10000, Croatia
E-mail: dks@phy.hr; nbarisic@phy.hr

The ORCID identification number(s) for the author(s) of this article can be found under https://doi.org/10.1002/adfm.202500099



**DOI: 10.1002/adfm.202500099**

L. Akšamović, N. Barišić
Institute of Solid State Physics
TU Wien
Vienna 1040, Austria

J. R. Soh
Quantum Innovation Centre (Q.InC)
Singapore Agency for Science Technology and Research
Singapore 138634, Singapore

K. Komędera, W. Tabiś
AGH University of Krakow
Faculty of Physics and Applied Computer Science
Kraków 30-059, Poland

K. Komędera
Mössbauer Spectroscopy Laboratory
Institute of Technology
University of the National Education Commission
Kraków 30-084, Poland

I. Biało
Physik-Institut
Universität Zürich
Zürich CH-8057, Switzerland

N. K. Chogondahalli Muniraju
Institute of Nuclear Physics PAN
Kraków 31-342, Poland

orbitals, the physical functionality of these materials often relies on the presence of open orbitals. This interplay creates a continuum of possibilities, ranging from insulating to highly conductive states. In particular, insulators are prized for their magnetic and optical properties, while conductors are studied for their potential to minimize energy dissipation, e.g., by superconductivity or by topologically protected surface states.

By investigating these materials, scientists hope to develop a deeper understanding of how emergent phenomena manifest and how they can be harnessed for technological applications. The study of emergent order not only provides insights into fundamental physics but also advances materials science and engineering.

The functionality of magnetic insulators typically depends on the open *d* orbitals of transition metal ions, a classic example being the ferrimagnetism observed in magnetite ($Fe^{2+}Fe_2^{3+}O_4$). In magnetite, not all iron atoms are in the same oxidation state, leading to an interplay between structural and local electronic properties.[8,9]

In this work, we explore the antiferromagnetic-like order observed in murunskite ($K_2FeCu_3S_4$), a quasi-two-dimensional (2D) semiconductor with a relatively simple structure.[10] Despite this simplicity, murunskite challenges the conventional understanding of magnetism in insulators, which often assumes a direct correlation between the crystal structure and the location of magnetic moments.

Murunskite occupies a unique position among functional materials, acting as an intermediary between high-temperature superconducting cuprates and pnictides. In cuprates, superconductivity arises from charge transfer between copper 3*d* orbitals and ligand oxygen 2*p* orbitals,[11,12] creating a localized hole within a "CuO4 molecule." This phenomenon plays a crucial role in both normal and superconducting states.[13–16] Conversely, in pnictides, the unit cell structure is defined by arsenic ligand orbitals bound with iron $e_{2g}$ suborbitals, which remain closed and distant from the Fermi level. The metallic properties[16,17] of pnictides result from the overlap of correlated $t_{2g}$ suborbitals on neighboring iron ions,[15,18–20] influenced by spin correlations from Hubbard repulsion.[21,22]

T. Ivšić
Department of Physical Chemistry
Ruđer Bošković Institute
Zagreb 10000, Croatia
O. Zaharko
Paul Scherrer Institut
Viligen CH-5232, Switzerland
C. Ritter
Institut Laue-Langevin
Grenoble 38000, France
T. LaGrange
Laboratory for Ultrafast Microscopy and Electron Scattering
École Polytechnique Fédérale de Lausanne
Lausanne CH-1015, Switzerland
L. Forró
Stavropoulos Center for Complex Quantum Matter
University of Notre Dame
IN 46556, USA
E-mail: lforro@nd.edu

Murunskite was synthesized via a novel pathway that yielded large high-quality single crystals, which enabled comprehensive material characterization, summarized in **Figure 1**.[10] This compound features a cleavable, layered structure, as illustrated in Figure 1a,b. Within the highly ordered *ab*-plane, Fe and Cu atoms are randomly distributed, as presented in transmission-electron microscopy (TEM) images shown in Figure 1c, with compositional analysis details in Supplement Section S1. The electrical resistivity of murunskite displays single-activated behavior, indicating no impurity states (Figure 1d). The material's electrical properties show significant anisotropy, with resistivity in the interlayer direction about 15 times higher than in-layer, reflecting its anisotropic structure (inset to Figure 1d). Furthermore, murunskite undergoes an antiferromagnetic (AFM) transition, clearly manifested by a distinct peak in the heat capacity at 97 K (Figure 1f), and corroborated by magnetic susceptibility data (Figure 1e), confirming the presence of long-range magnetic order. In murunskite, the metal sites are connected by sulfur ligand 2*p* orbitals, which are partially open even in the insulating parent compound. This electronic similarity to cuprates, despite structural similarities with pnictides, presents a unique situation where the ligand orbitals contribute to the material's electronic properties, making murunskite an intriguing subject for further study in the context of both superconductivity and magnetism.

The important finding of the present study is that murunskite exhibits nearly commensurate magnetic order at 97 K, even though positions and oxidation states of the iron atoms in the crystal lattice are disordered. This phenomenon indicates that the magnetism in murunskite is significantly characterized by emergent order, making it a distinctive subject for studying next-generation magnetic materials. Unlike typical scenarios, where real-space disorder is a secondary consideration, in murunskite it plays a pivotal role and must be accounted for from the outset.

The similarity between murunskite and high-entropy alloys (HEAs)[23–26] is intriguing. In both cases, there is a crystalline lattice with substantial site disorder, resulting in high lattice entropy. For HEAs, the central question revolves around how coherent wave propagation is possible amidst *structural* disorder. In murunskite, the key question is how long-range *magnetic* order can be established in a lattice where magnetic and nonmagnetic ions are randomly distributed. This parallel highlights the complexity and uniqueness of murunskite's magnetic properties, suggesting that further exploration of such materials could lead to new insights and advancements in magnetic and superconducting technologies.

The key challenge is understanding how the random distribution of magnetically active $Fe^{2+}$ and $Fe^{3+}$ ions—occupying only a quarter of the sites, with the remaining three-quarters filled by the closed-shell non-magnetic $Cu^{+}$ ions (typical for simple copper chalcogenides[27])—does not disrupt either the structural or magnetic order. To explore this, the study first revisits previously published data on murunskite's electronic and crystal structure using XPS, resistivity and magnetic susceptibility measurements in Figure 1 and Supporting Information. It then presents new findings from neutron diffraction and Mössbauer spectroscopy. It is suggested that relatively long-range magnetic interactions, extending up to second-neighbor couplings among iron atoms, may play a significant role. These highlight the potential involvement of sulfur ligands in maintaining the observed order. The

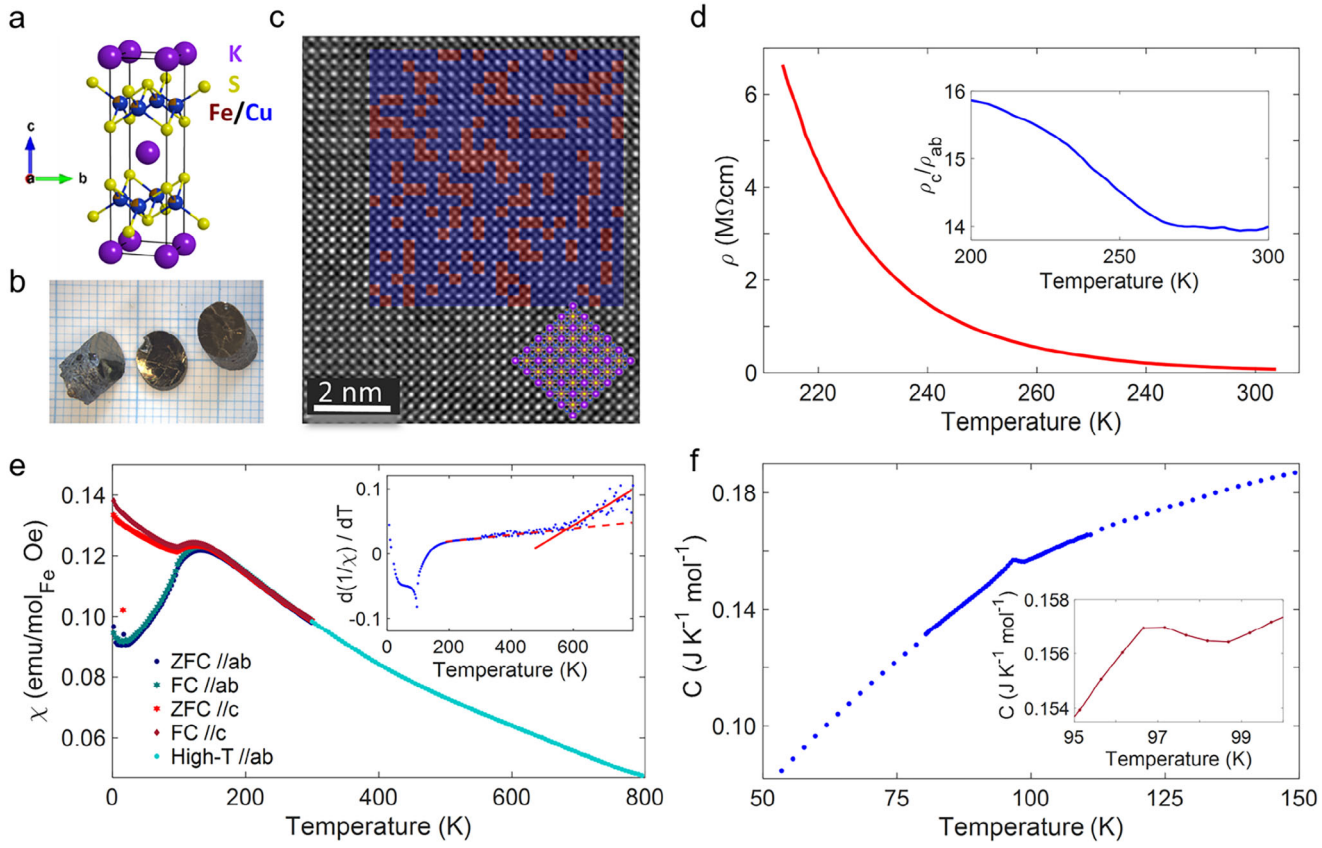


**Figure 1.** Structure and key microscopic properties of murunskite. a) Crystal structure of murunskite, where iron and copper (Cu) atoms occupy the same crystallographic positions in the ratio 1:3. The mixed occupancy of these two elements in the lattice is indicated by red and blue, respectively. b) Photo of murunskite single crystals on millimeter paper background; c) Atomic-resolution TEM image of murunskite, captured using a high-angle annular dark field (HAADF) detector. The top right overlay displays a simulated random distribution of Fe and Cu atoms (represented in red and blue, respectively) within a single layer, corresponding to the random occupation observed experimentally. The bottom right includes a 5x5 unit-cell overlay aligned parallel to the c-axis, highlighting the periodicity of the crystal structure. d) The temperature dependence of the electrical resistivity in the ab-plane, showing an activated semiconducting behavior. The inset shows the ratio of c-axis and ab-plane resistivities as a function of temperature. e) Temperature dependence of the magnetic susceptibility with an applied magnetic field (H) of 1 T, using both field-cooled (FC) and zero-field-cooled (ZFC) protocols measured using a Magnetic Property Measurement System (MPMS) for temperatures below 300 K (dark blue) and a Vibrating Sample Magnetometer (VSM) for temperatures above 300 K (light blue). The inset illustrates the derivative of the magnetic susceptibility as a function of temperature, with red lines serving as visual guides. The solid line indicates a noticeable change in slope above 550 K, suggesting changes in the magnetic interactions. f) Heat capacity of murunskite as a function of temperature. A prominent peak, highlighted in the inset, is observed around the antiferromagnetic (AFM) transition temperature indicating a phase transition.

study concludes by proposing that isolating local multi-centric wave functions as emergent building blocks could be a promising paradigm for development and interpretation of new functional materials. In that way, we lay the groundwork for understanding the mechanism responsible for full orbital order at even lower temperatures. Finally, these novel insights and approach may shed light on how emergent properties arise from disordered systems, how local interaction affects the properties of functional materials (e.g., cuprates), and open new possibilities for applications in material science.

## 2. Refinement of Magnetic Order

The random distribution of magnetic iron atoms in the $3d^{10}$ copper matrix of murunskite presents a compelling question: how do the spins organize in such a system? To explore this and to investigate the microscopic nature of the magnetic anomalies observed in the magnetometry data further, both powder and single-crystal neutron diffraction were measured on murunskite.

The neutron diffraction data and Rietveld refinement results for three distinct temperatures are shown in **Figure** 2a–c. In the paramagnetic regime, the neutron powder diffraction (NPD) data were refined considering only the lattice contributions (Figure 2a). At 150 K, an onset of short-range correlations was detected, characterized by a broad diffuse scattering peak centered around $2\theta = 15°$ (see Figure S3c, Supporting Information). Figure 2b highlights a portion of the NPD data and refinements at 110 K, emphasizing the short-range order diffuse scattering peak. As the temperature decreases from 110 K, the intensity of the diffuse scattering peak diminishes, and several new Bragg peaks emerge below 100 K, indicating the formation of long-range magnetic order. Notably, two Bragg peaks at low angles clearly appear

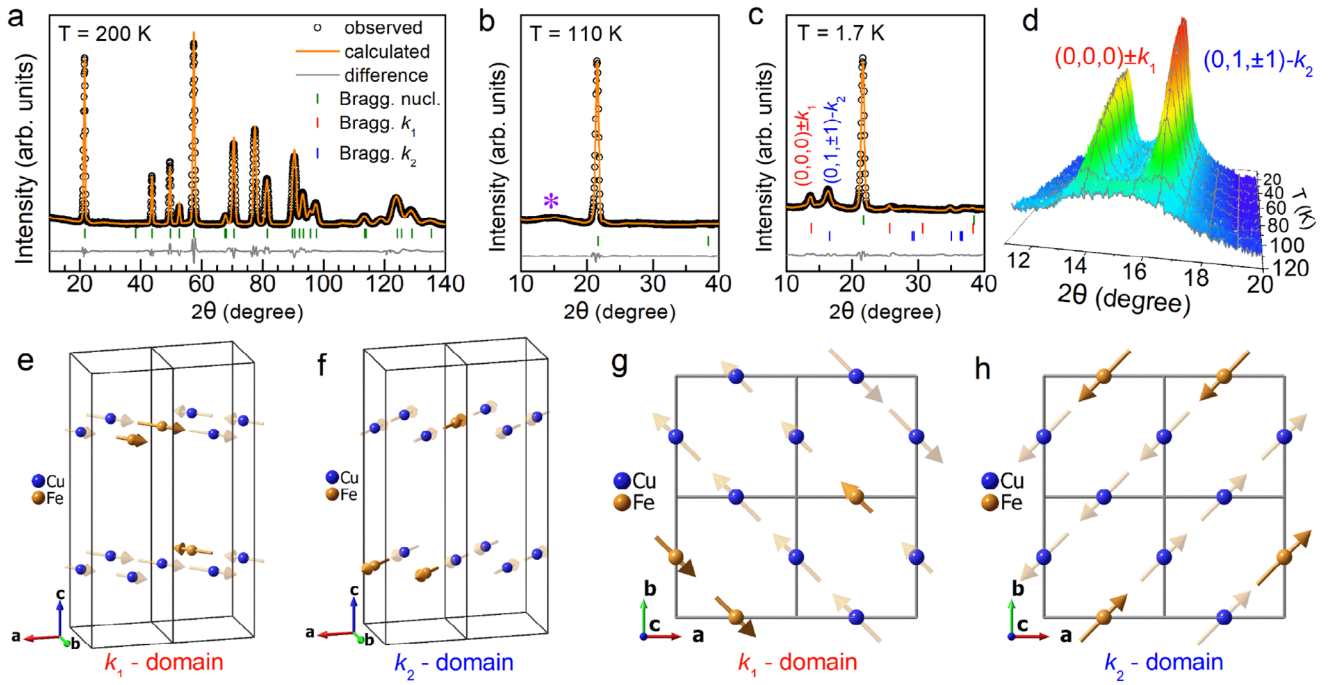


**Figure 2.** Neutron Powder Diffraction Analysis. a–c) NPD data and Rietveld refinement results are displayed for three representative temperatures: 200 K, 110 K, and 1.7 K. a) 200 K: The observed data could be refined using only the crystal lattice contribution. All diffraction peaks correspond to the expected Bragg positions for the lattice with the space group I4/mmm, implying no magnetic order at this temperature. b) 110 K: The data and refinements are similar to those at 200 K, with the addition of a broad diffuse scattering peak centered around $2\theta \approx 15°$ due to the emergence of short-range magnetic order. c) 1.7 K: The refinement was conducted assuming two equally populated magnetic domains with propagation vectors $k_1$ and $k_2$. The best magnetic superspace groups (MSSGs) for these domains are described in the main text, revealing long-range magnetic order. d) A contour plot of the low-angle portion of NPD data showing the temperature evolution of the diffuse scattering peak and the two main magnetic peaks associated with the magnetic domains characterized by propagation vectors $k_1$ and $k_2$. This plot illustrates the transition from short-range to long-range magnetic order as the temperature decreases. e–h) Graphical representations of spin arrangements derived from the Rietveld refinements. These diagrams show the spin configurations within $2 \times 1 \times 1$ and $2 \times 2 \times 0.5$ crystallographic unit cells for the two magnetic domains. The diagrams illustrate how the spins align differently in each domain, contributing to the overall magnetic structure observed in murunskite. Note that the closed-shell Cu (blue) is non-magnetic, so the spins (shown with faded yellow arrows) and its orientation, deduced from neutron data refinement, are plotted only to clearly illustrate the k-vectors for the arrangement of the Fe spins (yellow), despite their not being present on Cu sites.

atop the diffuse scattering peak. As the temperature continues to drop, the intensity of these new Bragg peaks increases, eventually saturating around 40 K.

Figure 2d illustrates the temperature-dependent behavior of NPD data surrounding the diffuse scattering peak within the temperature range of 110–1.7 K. This data captures the three main features associated with the evolution of magnetism with temperature: the short-range diffuse scattering peak, the onset of long-range order with two main magnetic peaks below 100 K, and the saturation of these magnetic peaks around 40 K. It is also worth noting that the magnetic susceptibility data in Figure 1d begins to deviate from the Curie–Weiss law at approximately 150 K, coinciding with the onset of the diffuse scattering peak in the NPD data at the same temperature. This correlation suggests a direct link between the observed magnetic anomalies and the orbital changes in murunskite.

Neutron diffraction on a single crystal in 4-circle mode allowed us to locate and index the Bragg peaks within the parent lattice setting of I4/mmm: $k_1$ = (0.25, 0.25, 0) [$k$-point ($aa$0)] and $k_2$ = (0.25, 0.75, 0) [$k$-point ($a1 - a$0)]. The profile fitting procedure of neutron powder diffraction data using the $k$-vectors obtained from single crystals did not match the observed pattern, but a good fit was obtained assuming two close but different incommensurate propagation vectors $k_1$ = (0.266(3), 0.266(3), 0) and $k_2$ = (0.24(2), 0.76(2), 0) = (0.24(2), 1 − 0.24(2), 0).

We resolved the magnetic structure using these two k-vectors, which could represent either a single magnetic domain with two propagation vectors or two magnetic domains with a single propagation vector. As neutron diffraction alone cannot distinguish between these scenarios, we used a two-domain, single-k approach to determine the magnetic structure, assuming equal populations of the $k_1$ and $k_2$ magnetic domains. Details of the symmetry analysis and all possible magnetic superspace groups (MSSG) associated with these domains are provided in Section S2 (Supporting Information).

To determine the incommensurate (IC) magnetic structures, we employed the Mag2pol program for a detailed Rietveld refinement of the NPD diffraction pattern, considering four possible MSSGs for the $k_1$ domain and two possible MSSGs for the $k_2$ domain. The best fits to the experimental data were obtained with MSSGs Fmmm.1'(0,0,g)s00s (irrep: mDT3, mk7t4) and B2/m.1'(a,b,0)00s (irrep: mC1, mk2t1). The refinements, shown in Figure 2c, indicate that the magnetic moments are primarily in-plane, with negligible c-components.

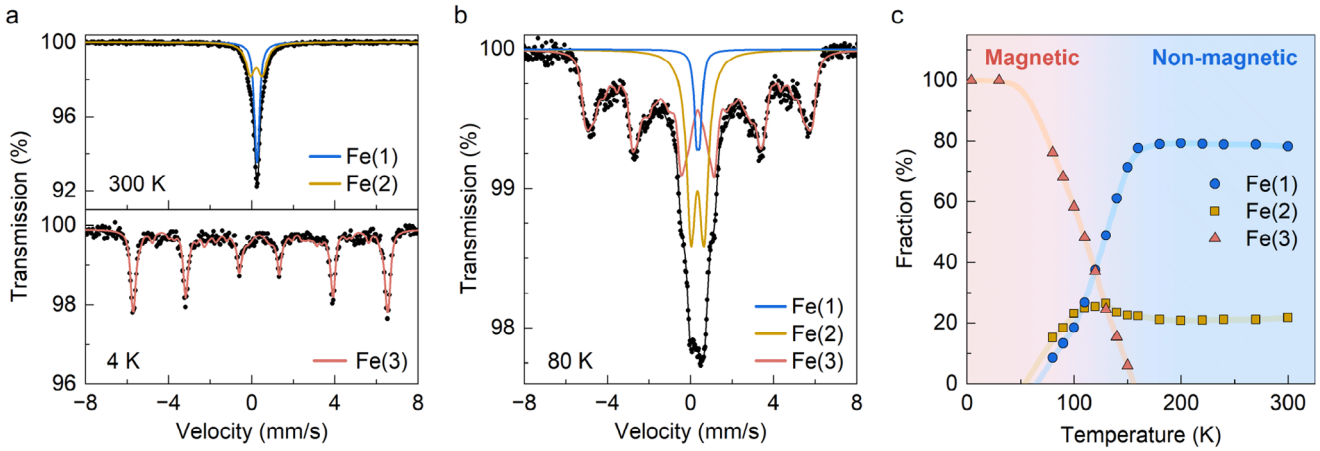


**Figure 3.** $^{57}$Fe Mössbauer Spectra Analysis. a) 300 K and 4K: Mössbauer spectra are displayed with the experimental data represented by black dots. The solid lines indicate the fit to the experimental data, with blue and yellow lines representing the two paramagnetic Fe sites [Fe(1) and Fe(2), respectively], and the red line representing the magnetic Fe site [Fe(3)]. b) 80 K: The same fitting conventions are applied, with the solid lines corresponding to the same three iron sites. c) Temperature-dependent contribution from each of the nonequivalent Fe sites. The colors of the solid points match the lines used in the fittings in panels (a) and (b). The shaded lines serve as visual guides, helping to track the changes in the fractions of the Fe sites as the temperature varies. The data shows how the contributions from paramagnetic sites [Fe(1) and Fe(2)] decrease with decreasing temperature, while the contribution from the magnetic site [Fe(3)] increases, reaching 100% at lower temperatures.

In the $k_1$ domain, the nearest-neighbor spins along the c direction are arranged in parallel, while they are antiparallel in the $k_2$ domain. From the refinements, the total amplitude of magnetic moment per $Fe^{2+}$ was found to be $3.02(7)\mu_B$ and $3.06(3)\mu_B$ in $k_1$ and $k_2$ domains, respectively at 1.7 K. This indicates that the moments have similar total amplitude in both domains despite the differences in magnetic modulations.

Significantly, the faded arrows in Figure 2e–h do not correspond to any local physical entity. The refinement determines the average magnetic moments per Wyckoff site without distinguishing between Cu and Fe. TEM measurements, single-crystal XRD, and high-temperature neutron data all confirm that 3/4 of the 4d Wyckoff sites are randomly occupied by nonmagnetic $Cu^+$ ions, while the remaining Fe ions are predominantly in the 2 + state, with some in the 3 + state, scattered randomly throughout the lattice. The critical question for murunskite's magnetism, similar to iron-pnictides, is the nature and location of these physical magnetic moments—whether they are local (orbital) moments or spin-density waves. To investigate it further, we turned to Mössbauer spectroscopy.

## 3. Orbital Evolution Revealed by Mössbauer Spectroscopy

The fitted Mössbauer spectra at various characteristic temperatures, along with the temperature dependence of the observed fractions of iron sites, are shown in **Figure 3**. The temperature-dependent Mössbauer data align well with magnetization and heat capacity measurements, revealing two paramagnetic sites above 150 K and one magnetic site emerging below this temperature in the murunskite powder sample.

The proportions of the two paramagnetic sites are approximately 80:20, remaining nearly constant until the third, magnetic site appears around 150 K, coinciding with the onset of short-range magnetic ordering revealed by magnetic susceptibility (Figure 1f) and neutron data (Figure 2d). Below this temperature, the fraction of the larger paramagnetic site gradually decreases, while the smaller one remains stable until the transition to long-range order at 97 K, after which both fractions decrease steadily. Meanwhile, the fraction of the magnetic site increases monotonically, reaching 100% between 30 and 60 K. This observation indicates that all iron sites become equivalent and fully magnetically ordered at low temperatures, despite the random distribution of local moments with two different valence states. It is consistent with neutron powder measurements, which show magnetic peak intensities saturating around 40 K (Figure 2d).

The observation of a unique magnetic site seems to favor the possibility of a multi-*k* vector structure over a multidomain structure. However, because Mössbauer spectroscopy is not sensitive to the microscopic origin of the long-range magnetic field, and simulations naturally produce a multidomain structure, the latter is preferred in the Discussion.

We benchmark the measured ratios of distinct sites by a random distribution of Fe and Cu atoms, to obtain the expected prevalence of various environments for the iron atoms. This simple statistical analysis suggests that 28% of iron atoms have only copper as their closest neighbors, while 6% have three or four Fe neighbors. However, Fe ions with four Fe neighbors are not preferred and are not stable, as seen in the end compound $K_{0.8}Fe_{1.6}S_2$, where partial occupation of K and Fe positions stabilizes the structure.[28] On the other hand, XPS measurements indicate that at most one-third of Fe ions are in the 3 + state. Then the simplest hypothesis is that Fe ions surrounded by only Cu neighbors are in the $Fe^{3+}$ state, while those with mixed neighbors are in the 2 + state. Moreover, because we expect some short-range correlations between Fe positions, given the importance of Fe dimers revealed by simulations below, it is most reasonable to assign the 80% fraction in Mössbauer spectroscopy to the $Fe^{2+}$ ions, and the 20% fraction to $Fe^{3+}$ ions.

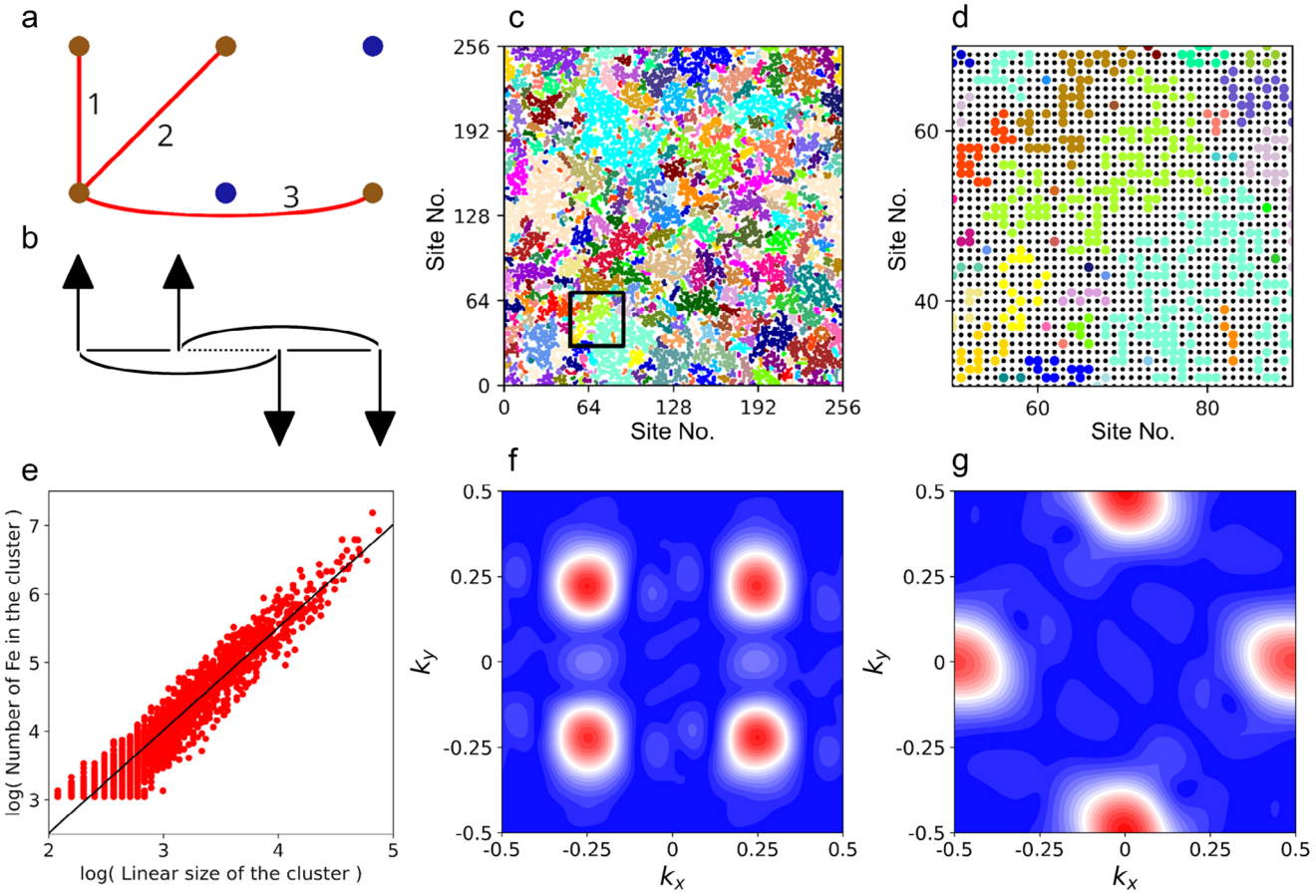


**Figure 4.** Magnetic and Structural Analysis of Murunskite. a) Spin–spin interactions attributed to sites both occupied by Fe atoms, where the first-neighbor interaction $J_1 > 0$ and both second-neighbor interactions $J_{2,3} < 0$. b) A quarter-zone configuration with two satisfied $J_1$ and $J_3$ bonds and one frustrated $J_1$ bond, with total energy $-J_1 + 2J_3$. c) Magnetic clusters in a 256 × 256-sample simulation near $T_c$. The Fourier transform of a similar 1024 × 1024 pattern appears in panel (f). Distinct clusters of Fe ions percolating through any of the bonds in (a) are depicted in different colors. The empty spaces are non-magnetic Cu ions. The colored sites are 1/4 of all sites, even if they dominate visually because the dots are sized to touch as nearest neighbors. Black square: inset magnified in (d) reveals that each percolating cluster is like a tree of cracks in the non-magnetic background of Cu ions, shown as black dots. e) Scaling of the number of Fe atoms vs. linear size (side of enveloping square) of a cluster, showing a fractal dimension of 1.50 for clusters with more than 20 Fe atoms. The regression line is $(1.5001 \pm 0.0092)x - 0.4856 \pm 0.0280$. f) Fourier transform of a simulated spin distribution for $J_2 = J_3 = -1.5J_1$. Compare the real-space pattern in panel (c). g) Fourier transform of a distribution with $J_2 = -1.5J_1$ and $J_3 = 0$. Units of $2\pi/a$.

The dominant paramagnetic site (site 1) in Mössbauer spectroscopy is sensitive to the onset of short-range order, while the minority paramagnetic site (site 2) responds only to long-range order. Both paramagnetic sites are depleted in favor of the single magnetic site (site 3). It is inferred that $Fe^{2+}$ ions (with mixed neighbors) initiate ordering fluctuations at 150 K, while $Fe^{3+}$ ions contribute to the magnetic order only when it becomes long-range. It remains an open question whether the saturation of the magnetic site at 100% below 40 K corresponds to an $Fe^{3+} \rightarrow Fe^{2+}$ orbital transition, indicating that all magnetic sites belong to a single orbital state at very low temperatures (further details in Section S3, Supporting Information).

## 4. Simulations

In disordered alloys, the Brillouin zone of the parent lattice can persist in angle-resolved photoemission spectroscopy even when alloying disrupts translational invariance.[29] The disruption primarily affects the widths of the peaks in reciprocal space, which retain some intensity as long as the material is not structurally amorphous. We observe a similar phenomenon in the magnetic properties of murunskite, documented here for the first time. To substantiate this observation, we conducted simulations, with details in Section S4 (Supporting Information).

Starting with a random distribution of Fe atoms, we attributed spin-spin interactions according to the model in **Figure** 4a, connecting Fe atoms with red lines. The resulting Heisenberg Hamiltonian was solved in the mean-field approximation on a lattice of 1024 × 1024 sites.

Density functional theory (DFT) calculations in large supercells were performed to narrow down the coupling constants. We estimate them by calculating the formation energy of the various configurations in Figure 4a by methods developed for point defects.[30] The calculations indicate that $J_1$ must be ferromagnetic, leading to the formation of magnetic dimers with large moments, roughly double that of the $Fe^{2+}$ ions, which are found

in the output of the calculation. This explains the high magnetic moment observed in magnetic susceptibility measurements.[10] $J_2$ was similarly found to be negative. We could not include $J_3$ due to supercell size limitations, because the linear arrangement of pairs of Fe atoms interacting by $J_3$ induces artefacts of ordered Fe chains, which can be avoided only in very large cells (at least 160 atoms). However, our simulation results suggest unequivocally that $J_3$ must be similar in magnitude and sign to $J_2$ (see Supporting Information). With these parameters, our simulation reproduced the neutron scattering data successfully, indicating nearly quarter-zone peaks with variations in position between 0.24 and 0.27 on either axis, depending on the random distribution of Fe sites.

A qualitatively different Fourier pattern emerged when $J_3$ was set to 0, as shown in Figure 4g. This robustly infers the presence of significant second-neighbor coupling in murunskite, in contrast to the half-zone magnetic responses typically seen in ferropnictides, where all lattice sites are occupied by magnetic Fe atoms.

The simulation also provided a critical temperature $T_c \approx 4.8J_1$, corresponding to $J_1 \approx 0.002$ eV, much smaller than superexchange interactions in cuprates[12] or antiferromagnetic pnictides.[31] This discrepancy can be attributed to the absence of quantum fluctuations in our simulations and the lower energy differences and greater covalency of sulfur orbitals in murunskite. The high-temperature magnetic susceptibility data (Figure 1d) shows a change in slope around 550 K, likely corresponding to the dissociation of Fe–Fe dimers, indicating a microscopic $J_1$ similar to that in antiferromagnetic pnictides.

Previous DFT calculations showed that sulfur orbitals in murunskite are partially open even in the insulating state, with small spin polarization.[10] These orbitals serve as conduits for magnetic correlations, which must extend at least to the second neighbors to account for the observed data.

Concerning the possible effect of fluctuations on our mean field results, the effect of 2D infrared fluctuations in an extreme anisotropic case of the Heisenberg model, the XXZ model, has been analyzed recently in the context of the Hohenberg–Mermin–Wagner theorem.[32] It was found that fluctuations that prevent 2D order can themselves be efficiently suppressed by any number of mechanisms. If multiple mechanisms breaking continuous symmetry act simultaneously—such as disorder, perpendicular coupling, and finite size—the mechanism which yields the highest restored $T_c$ will prevail (not the lowest, as intuition would suggest). Based on this work, we can confidently conclude that the disorder in Fe positions, combined with relatively strong $J_1$, $J_2$ and $J_3$ bonds, makes the mean-field approach sufficiently reliable to support the experimental results. Notably, these results clearly reveal a ~100 K phase transition despite the compound's electronic and structural two-dimensionality. In particular, the small magnetic islands into which our system fragments inherently constrain long-wavelength fluctuations of the order parameter. More broadly, when a mean-field description aligns with experimental observations, incorporating fluctuations should not alter the overall picture fundamentally.

## 5. Discussion and Conclusion

The study of murunskite reveals that its magnetic and orbital order emerges in a crystal structure characterized by a complete disorder in the positions of mixed-valence Fe ions, which occupy 1/4 of the available tetrahedral sites, with the remaining 3/4 being filled by non-magnetic $Cu^+$ ions.[10] Despite this disorder, the magnetic responses are notably regular, with calorimetry, neutron scattering, and Mössbauer spectroscopy all indicating an AF-like transition at 97 K and a single ordered site at low temperatures (≈40 K).

A dedicated statistical simulation shows that real-space disorder can be absorbed into peak widths in inverse space, akin to the result for disordered alloys, but in the magnetic sector. This concept aligns well with the neutron scattering data, despite the lack of local distortions typical of high-entropy alloys. The Mössbauer and XPS data provide further nuance, indicating two distinct paramagnetic sites at high temperatures, which transition into a single magnetic site below 97 K. The emergence of this ordered site likely results from a combination of local environments and oxidation states of Fe atoms.

The simulation indicates that magnetically ordered islands form near the AF transition temperature, with their size and interaction becoming extended below 40 K. Mössbauer spectroscopy is consistent with a conjectured gradual orbital transition from $Fe^{3+}$ to $Fe^{2+}$, contributing to the long-range magnetic order. This scenario parallels the behavior observed in cuprates, where an orbital crossover which delocalizes doped holes significantly affects the materials' superconductivity.[15]

The magnetism in murunskite differs significantly from that in pnictides, primarily due to the real-space disorder of magnetic Fe ions. In cuprates, the situation is more similar, because doping introduces such disorder in the magnetic sector. Feedbacks between the magnetic, orbital, and lattice degrees of freedom are relevant for all functional materials. Murunskite is exceptional in that the lattice is apparently not importantly involved despite compositional Fe/Cu disorder. Decoupling of the lattice from (conventional) magnetism has been observed in manganese containing quaternary sulfosalt, however without in-depth analysis of its crystal and magnetic structure.[33] The presence of ferromagnetically coupled $Fe^{2+}$ dimers and the involvement of partially open S-ligand 2*p* orbitals suggest a unique magnetic interaction mechanism, reminiscent of molecular magnets, rather than traditional superexchange-mediated AF insulators.

From the standpoint of fundamental quantum mechanics, the intrinsic interest of magnetic order in complex materials is on par with phenomena such as superconductivity. In particular, our investigation of murunskite suggests that wave functions coherent across multiple unit cells play a significant role. A three-site structure has previously been inferred along similar lines in magnetite.[9] Furthermore, a very high degree of magnetic isolation of spin chains has been observed in some Haldane $S = 1$ molecular materials,[34] without the topological protection found in others.[35] Finally, magnetism in organic crystals indicates coherence among large molecules across distances that surprisingly exceed those we learned to expect from simpler structures.[36,37] In this context, murunskite has an unexpected combination of magnetic complexity and structural simplicity, possibly related to the electronic malleability of the sulfur ligands.

The discovery of robust AF order within small, tree-like magnetic patches in a disordered environment highlights the potential for designing new materials with similar properties. The small size of these islands, which is decoupled from the lattice

details, suggests possibilities for applications in nanostructuring, including the manipulation of island sizes via impurities or substrate effects. This finding indicates that multi-centric wave functions involving the partially open S-ligand 2*p* orbitals are the basic building blocks of the clusters. The ease of cleaving the material, combined with the emergence of full orbital and spin order despite strong inherent disorder, also points to potential 2D applications, such as thin films, where recent fundamental insights show that low dimensionality need not hinder ordering.[32]

In conclusion, murunskite displays emergent long-range magnetic and orbital order despite significant site and high-temperature orbital disorder among its magnetic ions. This behavior can be understood as a magnetic analogue of a disordered alloy, with magnetic interactions mediated by functionalized sulfur orbitals. The presence of a mesoscopic cluster structure and a possible orbital transition of Fe ions are key areas for further experimental investigation.

## 6. Experimental Section

Single crystals of murunskite were grown using a two-step synthesis method as previously reported.[10] Initially, iron copper sulfide was synthesized from elemental components through a solid-state reaction. Subsequently, elemental potassium was added, and single crystals were grown from the melt by slow cooling. The following measurements and analyses were performed on large high-quality single crystals:

*Powder Neutron Diffraction*: Measurements were conducted on the D20 beamline at the Institut Laue Langevin (ILL) in Grenoble. Approximately 1.1 g of powder was placed in a vanadium container and measured using a wavelength of 2.4 Å. The high-intensity 2-axis diffractometer, equipped with a large microstrip detector and operating at extremely high neutron flux, enabled full powder diffraction measurements at a base temperature, as well as temperature-dependent studies over an interesting range.

*Single Crystal Neutron Diffraction*: A large murunskite single crystal ($6 \times 7 \times 4$ mm$^3$) was analyzed using the ZEBRA instrument at the Paul Scherrer Institut (PSI) in Villigen. The measurements were conducted in a 4-circle mode with both short (1.18 Å) and long (2.32 Å) wavelengths, utilizing a point detector and a 160 mm × 160 mm area detector, which facilitated reliable determination of k-vectors.

*Mössbauer Spectroscopy*: Mössbauer spectra were recorded at the Mössbauer setup at the University of Krakow, Poland, to determine the local Fe environment and magnetic structure of murunskite. The spectra were collected in standard transmission geometry for the 14.41 keV transition in 57Fe using a 57Co(Rh) source at ambient pressure and room temperature. The absorbing sample was prepared by mixing 30 mg of murunskite powder with a B4C carrier, resulting in an absorber thickness of 14.9 mg cm$^{-2}$. Temperature control was maintained using a Janis Research Co. SVT-400 cryostat, with a long-term accuracy of better than 0.01 K (except at 4.2 K, where accuracy was better than 0.1 K). A RENON MsAa-4 Mössbauer spectrometer equipped with a Kr-filled proportional counter was used to collect the spectra in the photo-peak window. The velocity scale of the spectrometer was calibrated using a Michelson-Morley interferometer with a He-Ne laser. Spectral shifts are reported relative to natural $\alpha$-Fe at ambient pressure and room temperature. The spectra were fitted using the transmission integral approximation with the Mosgraf-2009 software.[38]

*Symmetry Analysis*: Symmetry analysis was performed using ISODISTORT from the ISOTROPY software suite,[39,40] along with tools from the Bilbao Crystallographic Server.[41,42] The Rietveld refinement of neutron powder diffraction data was carried out using the Mag2pol program,[43] leveraging its internal tables for neutron scattering lengths to determine crystal and magnetic structure parameters.

*DFT Calculations*: The Quantum ESPRESSO package was used,[44,45] with the PBESOL exchange-correlation functional.[46,47] Pseudopotentials were taken from.[48] The kinetic energy cutoffs were 80 Ry for wavefunctions, and 600 Ry for charge density and potentials. The Brillouin zone sampling was 8x8x5 with no shift for a 40-atom supercell. The DFT+U approach was according to.[49] The Hubbard interaction for the Fe 3d orbitals was 3.7606 eV, and 4.0 eV for Cu 3d, calculated according to.[50]

## Supporting Information

Supporting Information is available from the Wiley Online Library or from the author.

## Acknowledgements

The work at the University of Zagreb was supported by project CeNIKS co-financed by the Croatian Government and the European Union through the European Regional Development Fund Competitiveness and Cohesion Operational Program (Grant No. KK.01.1.1.02.0013), the Croatian-Swiss Research Program of the Croatian Science Foundation and the Swiss National Science Foundation with funds obtained from the Swiss-Croatian Cooperation Program Project No. IZHRZ0-180652, the Swiss National Science Foundation through grant No. 200021-175836, and by the Croatian Science Foundation under Project No. IP-2022-10-3382. The work at AGH University was supported by the National Science Centre, Poland, Grant OPUS: 2021/41/B/ST3/03454; the Polish National Agency for Academic Exchange under "Polish Returns 2019" Programme No. PPN/PPO/2019/1/00014; and the "Excellence Initiative-Research University" program for AGH University of Krakow. I. Biało acknowledges support from the Swiss Confederation through Government Excellence Scholarships. J.R acknowledges support from the Singapore National Science Scholarship, Agency for Science Technology and Research and the European Research Council (HERO, Grant No. 810451). We acknowledge Virgile Favre (ILL, D20, Proposal ID: 5-31-2772), Bachir Ouladdiaf (ILL, Cyclops, Proposal ID: EASY-1015) and Paola Caterina (PSI, Zebra, Proposal ID: 20220994) for their help with proposal preparation and acquisition of the neutron diffraction data. This research was funded in part by the Austrian Science Fund (FWF) [10.55776/F86; 10.55776/P35945]. For open access purposes, the author has applied a CC BY public copyright license to any author accepted manuscript version arising from this submission.

Open access funding provided by Technische Universitat Wien/KEM.

## Conflict of Interest

The authors declare no conflict of interests.

## Author Contributions

LF, HR, DKS, and NB conceived the project. Single crystals were synthesized by DT, PR, and TI. Magnetic susceptibility measurements were performed by DT, PR, and IZ, and analyzed by DT and IZ. Transport measurements were conducted by DT, PR, IZ, and MN. SEM/TEM measurements and analysis were performed by DT and TLG. Neutron diffraction was conducted by DT, JRS, IZ, and CR, and analyzed by DT, CMNK, OZ, and CR. Mössbauer spectroscopy was measured and analyzed by DT, KK, and WT. XPS/XAS experiments were carried out by DT, PR, LA, IB, and WT. Simulations and DFT calculations were carried out by IB. The principal interpretation lines were proposed by DKS and NB. The manuscript was written by DT, LF, DKS, and NB, with contributions from all authors.

## Data Availability Statement

The data that support the findings of this study are available from the corresponding author upon reasonable request.

## Keywords

experimental and DFT calculations, heterogeneous, local correlations, magnetic materials, superconductivity

Received: January 2, 2025
Revised: April 13, 2025
Published online: May 2, 2025

[1] E. Schrödinger, *What is life?: the physical aspect of the living cell; with Mind and matter; & Autobiographical sketches*, Canto. Cambridge University Press Cambridge, Cambridge **1992**.
[2] P. W. Anderson, *Science* **1972**, *177*, 393.
[3] K. M. Shen, J. S. Davis, *Mater. Today* **2008**, *11*, 14.
[4] T. Yoshida, M. Hashimoto, I. M. Vishik, Z.-X. Shen, A. Fujimori, *J. Phys. Soc. Jpn.* **2012**, *81*, 011006.
[5] Q. Si, R. Yu, E. Abrahams, *Nat. Rev. Mater.* **2016**, *1*, 16017.
[6] M. D. Lumsden, A. D. Christianson, *J. Phys.: Condens. Matter* **2010**, *22*, 203203.
[7] M. Hashimoto, I. M. Vishik, R.-H. He, T. P. Devereaux, Z.-X. Shen, *Nat. Phys.* **2014**, *10*, 483.
[8] J. P. Wright, J. P. Attfield, P. G. Radaelli, *Phys. Rev. Lett.* **2001**, *87*, 266401.
[9] M. S. Senn, J. P. Wright, J. P. Attfield, *Nature* **2012**, *481*, 173.
[10] D. Tolj, T. Ivšić, I. Živković, K. Semeniuk, E. Martino, A. Akrap, P. Reddy, B. Klebel-Knobloch, I. Lončarić, L. Forró, N. Barišić, H. M. Ronnow, D. K. Sunko, *Appl. Mater. Today* **2021**, *24*, 101096.
[11] J. Zaanen, G. A. Sawatzky, J. W. Allen, *Phys. Rev. Lett.* **1985**, *55*, 418.
[12] H. Eskes, J. H. Jefferson, *Phys. Rev. B* **1993**, *48*, 9788.
[13] N. Barišić, M. K. Chan, M. J. Veit, C. J. Dorow, Y. Ge, Y. Tang, W. Tabis, G. Yu, X. Zhao, M. Greven, *arXiv* **2015**.
[14] D. Pelc, P. Popčević, M. Požek, M. Greven, N. Barišić, *Sci. Adv.* **2019**, *5*, eaau4538.
[15] N. Barišić, D. K. Sunko, *J. Supercond. Novel Magn.* **2022**, *35*, 1781.
[16] C. M. N. Kumar, A. Akrap, C. C. Homes, E. Martino, B. Klebel-Knobloch, W. Tabis, O. S. Barišić, D. K. Sunko, N. Barišić, *Phys. Rev. B* **2023**, *107*, 144515.
[17] N. Barišić, D. Wu, M. Dressel, L. J. Li, G. H. Cao, Z. A. Xu, *Phys. Rev. B* **2010**, *82*, 054518.
[18] S. V. Borisenko, D. V. Evtushinsky, Z.-H. Liu, I. Morozov, R. Kappenberger, S. Wurmehl, B. Buchner, A. N. Yaresko, T. K. Kim, M. Hoesch, T. Wolf, N. D. Zhigadlo, *Nat. Phys.* **2016**, *12*, 311.
[19] G. Derondeau, F. Bisti, M. Kobayashi, J. Braun, H. Ebert, V. A. Rogalev, M. Shi, T. Schmitt, J. Ma, H. Ding, V. N. Strocov, J. Minár, *Sci. Rep.* **2017**, *7*, 8787.
[20] D. K. Sunko, *J. Supercond. Novel Magn.* **2020**, *33*, 27.
[21] H. Eschrig, K. Koepernik, *Phys. Rev. B* **2009**, *80*, 104503.
[22] J. Fink, S. Thirupathaiah, R. Ovsyannikov, H. A. Dürr, R. Follath, Y. Huang, S. de Jong, M. S. Golden, Y.-Z. Zhang, H. O. Jeschke, R. Valentí, C. Felser, S. Dastjani Farahani, M. Rotter, D. Johrendt, *Phys. Rev. B* **2009**, *79*, 155118.
[23] M.-H. Tsai, J.-W. Yeh, *Mater. Res. Lett.* **2014**, *2*, 107.
[24] D. Miracle, O. Senkov, *Acta Mater.* **2017**, *122*, 448.
[25] Q. He, Y. Yang, *Front. Mater.* **2018**, *5*.
[26] S. Moniri, Y. Yang, J. Ding, Y. Yuan, J. Zhou, L. Yang, F. Zhu, Y. Liao, Y. Yao, L. Hu, P. Ercius, J. Miao, *Nature* **2023**, *624*, 564.
[27] J. Folmer, F. Jellinek, *J. Less Common Metals* **1980**, *76*, 153.
[28] H. Lei, M. Abeykoon, E. S. Bozin, C. Petrovic, *Phys. Rev. B* **2011**, *83*, 180503.
[29] V. Popescu, A. Zunger, *Phys. Rev. B* **2012**, *85*, 085201.
[30] C. Freysoldt, B. Grabowski, T. Hickel, J. Neugebauer, G. Kresse, A. Janotti, C. G. Van de Walle, *Rev. Mod. Phys.* **2014**, *86*, 253.
[31] J. Zhao, D. T. Adroja, D. Yao, R. Bewley, S. Li, X. F. Wang, G. Wu, X. H. Chen, J. Hu, P. Dai, *Nat. Phys.* **2009**, *5*, 555.
[32] G. Palle, D. K. Sunko, *J. Physics A: Mathemat. Theoret.* **2021**, *54*, 315001.
[33] A. Virtue, X. Zhou, B. Wilfong, J. W. Lynn, K. Taddei, P. Zavalij, L. Wang, E. E. Rodriguez, *Phys. Rev. Mater.* **2019**, *3*, 044411.
[34] R. C. Williams, W. J. A. Blackmore, S. P. M. Curley, M. R. Lees, S. M. Birnbaum, J. Singleton, B. M. Huddart, T. J. Hicken, T. Lancaster, S. J. Blundell, F. Xiao, A. Ozarowski, F. L. Pratt, D. J. Voneshen, Z. Guguchia, C. Baines, J. A. Schlueter, D. Y. Villa, J. L. Manson, P. A. Goddard, *Phys. Rev. Res.* **2020**, *2*, 013082.
[35] P. Tin, M. J. Jenkins, J. Xing, N. Caci, Z. Gai, R. Jin, S. Wessel, J. Krzystek, C. Li, L. L. Daemen, Y. Cheng, Z.-L. Xue, *Nat. Commun.* **2023**, *14*, 5454.
[36] H. Liu, H. Malissa, R. M. Stolley, J. Singh, M. Groesbeck, H. Popli, M. Kavand, S. K. Chong, V. V. Deshpande, J. S. Miller, C. Boehme, Z. V. Vardeny, *Adv. Mater.* **2020**, *32*, 2002663.
[37] S. H. Lapidus, P. W. Stephens, M. Fumanal, J. Ribas-Ariño, J. J. Novoa, J. G. DaSilva, A. L. Rheingold, J. S. Miller, *Dalton Trans.* **2021**, *50*, 11228.
[38] L. Duraj, K. Ruebenbauer, *Acta Phys. Pol. A* **2011**, *119*, 75.
[39] B. J. Campbell, H. T. Stokes, D. E. Tanner, D. M. Hatch, *J. Appl. Crystallogr.* **2006**, *39*, 607.
[40] H. T. Stokes, D. M. Hatch, B. J. Campbell, Isotropy software suite, **2021**, http://www.iso.byu.edu.
[41] M. I. Aroyo, J. M. Perez-Mato, D. Orobengoa, E. Tasci, G. de la Flor, A. Kirov, *Bulg. Chem. Commun* **2011**, *43*, 183.
[42] J. Perez-Mato, S. Gallego, E. Tasci, L. Elcoro, G. de la Flor, M. Aroyo, *Annu. Rev. Mater. Res.* **2015**, *45*, 217.
[43] N. Qureshi, *J. Appl. Crystallogr.* **2019**, *52*, 175.
[44] P. Giannozzi, S. Baroni, N. Bonini, M. Calandra, R. Car, C. Cavazzoni, D. Ceresoli, G. L. Chiarotti, M. Cococcioni, I. Dabo, A. Dal Corso, S. de Gironcoli, S. Fabris, G. Fratesi, R. Gebauer, U. Gerstmann, C. Gougoussis, A. Kokalj, M. Lazzeri, L. Martin-Samos, N. Marzari, F. Mauri, R. Mazzarello, S. Paolini, A. Pasquarello, L. Paulatto, C. Sbraccia, S. Scandolo, G. Sclauzero, A. P. Seitsonen, et al., *J. Phys.: Condens. Matter* **2009**, *21*, 395502.
[45] P. Giannozzi, O. Andreussi, T. Brumme, O. Bunau, M. Buongiorno Nardelli, M. Calandra, R. Car, C. Cavazzoni, D. Ceresoli, M. Cococcioni, N. Colonna, I. Carnimeo, A. Dal Corso, S. de Gironcoli, P. Delugas, R. A. DiStasio, A. Ferretti, A. Floris, G. Fratesi, G. Fugallo, R. Gebauer, U. Gerstmann, F. Giustino, T. Gorni, J. Jia, M. Kawamura, H.-Y. Ko, A. Kokalj, E. Küçükbenli, M. Lazzeri, et al., *J. Phys.: Condens. Matter* **2017**, *29*, 465901.
[46] J. P. Perdew, A. Ruzsinszky, G. I. Csonka, O. A. Vydrov, G. E. Scuseria, L. A. Constantin, X. Zhou, K. Burke, *Phys. Rev. Lett.* **2008**, *100*, 136406.
[47] J. P. Perdew, A. Ruzsinszky, G. I. Csonka, O. A. Vydrov, G. E. Scuseria, L. A. Constantin, X. Zhou, K. Burke, *Phys. Rev. Lett.* **2009**, *102*, 039902.
[48] A. Dal Corso, *Comput. Mater. Sci.* **2014**, *95*, 337.
[49] S. L. Dudarev, G. A. Botton, S. Y. Savrasov, C. J. Humphreys, A. P. Sutton, *Phys. Rev. B* **1998**, *57*, 1505.
[50] I. Timrov, N. Marzari, M. Cococcioni, *Comput. Phys. Commun.* **2022**, *279*, 108455.